Kobe University Repository : Kernel

PDF issue: 2025-12-05

Direct confirmation of the dopant site in indium-doped SrTiO3 photocatalyst via atomic-scale analytical transmission electron microscopy imaging

Kitta, Mitsunori
Taguchi, Noboru
Sudrajat, Hanggara
Onishi, Hiroshi

(Citation)
Applied Physics Letters,118(15):153901

(Issue Date)
2021-04-12

(Resource Type)
journal article

(Version)
Version of Record

(Rights)
© 2021 Author(s). Published under license by AIP Publishing. This article may be downloaded for personal use only. Any other use requires prior permission of the author and AIP Publishing. This article appeared in Appl. Phys. Lett. 118, 15, 153901 (2021) and may be found at at https://doi.org/10.1063/5.0047290

(URL)
https://hdl.handle.net/20.500.14094/90008904

KOBE UNIVERSITY

Applied Physics Letters ARTICLE scitation.org/journal/apl

Direct confirmation of the dopant site in indium-doped $SrTiO_3$ photocatalyst via atomic-scale analytical transmission electron microscopy imaging

Cite as: Appl. Phys. Lett. **118**, 153901 (2021); doi: 10.1063/5.0047290
Submitted: 11 February 2021 · Accepted: 26 March 2021 ·
Published Online: 12 April 2021

View Online Export Citation CrossMark

Mitsunori Kitta,[1,a] Noboru Taguchi,[1] Hanggara Sudrajat,[2,b] and Hiroshi Onishi[2]

AFFILIATIONS

[1]Research Institute of Electrochemical Energy, Department of Energy and Environment, National Institute of Advanced Industrial Science and Technology, 1-8-31, Midorigaoka, Ikeda, Osaka 563-8577, Japan
[2]Department of Chemistry, Graduate School of Science, Kobe University, 1-1 Rokkodai, Nada-ku, Kobe 657-8501, Japan

Note: This paper is part of the APL Special Collection on Materials for Renewable Fuels Production.
[a]**Author to whom correspondence should be addressed:** m-kitta@aist.go.jp
[b]**Present address**: Department of Chemical Engineering, Faculty of Engineering, Universitas Jember, Jember 68121, Indonesia.

ABSTRACT

Confirming the dopant site of In^{3+}-doped $SrTiO_3$ (In–STO) is essential to reveal the mechanism of its photocatalytic activity. In a previous study, x-ray absorption spectroscopic analysis and theoretical investigations were performed to discuss the dopant site, and In^{3+}–Ti^{4+} substitution was proposed. However, direct confirmation of the In^{3+} dopant site has not yet been reported. Here, we performed direct atomic-scale imaging of In–STO crystals via analytical transmission electron microscopy and revealed the dopant site based on real-space elemental mapping. The Ti and Sr sites in the $SrTiO_3$ crystal lattice were well identified by atomic column elemental mapping using energy dispersive x-ray spectroscopy (EDS). The EDS signal of indium has a stronger intensity at the Ti site than at the Sr site, based on the total analysis of each Ti and Sr atomic column. By applying principal component analysis on the raw EDS spectral imaging data cube, the indium site was clearly imaged; it completely fit into the Ti atomic column positions. These results provide direct evidence of In–Ti substitution in In-STO photocatalysts.

Published under license by AIP Publishing. https://doi.org/10.1063/5.0047290

Strontium titanium oxide ($SrTiO_3$) with a cubic perovskite structure (space group *Pm-3m*, No. 221) is well known as a photocatalyst for overall water splitting[1–3] and is a promising candidate as a hydrogen generation material by ultraviolet (UV) photon energy irradiation. Enhancement of $SrTiO_3$ photocatalyst activity has been the focus of research for producing hydrogen by sunlight irradiation. Recently, some specific metal cations as impurities elements that enhance the photocatalytic activity of $SrTiO_3$ via solid-solution formation have been reported.[4] To enhance the quantum yield of photocatalytic reaction, the amount of these impurities usually reaches to mol% level. Although the amount of impurities in semiconductor materials is mostly ppm order, here we defined these metal cation impurities as dopant, by meaning of photocatalytic research. Especially, indium cation (In^{3+}) doping, as well as Ga^{3+} and Al^{3+} doping, into the $SrTiO_3$ lattice enhances the activity.[5,6] This can be explained by the substitution of Ti^{4+} with O^{2-} vacancy[7] as follows:

$$2In^{3+} \Longleftrightarrow 2Ti^{4+}(\text{substitution}) + O^{2-}(\text{vacancy}). \quad (1)$$

Here, O^{2-} vacancy formation can enhance the photocatalytic activity of water splitting via charge separation.[8]

Alternatively, to charge compensate, In^{3+} substitution may also occur

$$2In^{3+} \Longleftrightarrow Sr^{2+}(\text{substitution}) + Ti^{4+}(\text{substitution}). \quad (2)$$

Here, Sr^{2+} substitution with In^{3+} should stabilize Ti^{3+} defects in the crystal lattice, decreasing photocatalytic activity.[7] Therefore, the substitution mechanism of In^{3+} into $SrTiO_3$ is significant for studying photocatalytic activity from the basis of the dopant engineering. To reveal the dopant site of indium-doped $SrTiO_3$ (In–STO) crystal, we previously studied via x-ray absorption fine structure analysis and density functional theory (DFT) calculations.[9] There, we concluded that dopant-site (Ti or Sr) is a main issue of photocatalytic activities,

Published under license by AIP Publishing

because it directly affects the band structure. The Sr–In substitution makes impurity state, originated from In–O hybridization, within the main bandgap. It should play a role to a recombination center for photogenerated electrons and holes. While the Ti–In substitution does not make such state, and it should be suitable for effective charge separation by photon irradiation. Therefore, direct confirmation of the dopant site is the main topic of photocatalytic science of In-STO photocatalyst. From the crystal model of $SrTiO_3$ shown in Fig. 1, one sees that Ti^{4+} has TiO_6 octahedral coordination, whereas Sr^{2+} has SrO_{12} cuboctahedral coordination. The oscillation feature of the extended x-ray absorption fine structure was close to that of the InO_6 octahedral coordination structure, suggesting Ti^{4+} substitution. Furthermore, the simulated band structure of the Ti^{4+}-substituted theoretical model explained the experimental optical absorption feature better than the Sr^{2+} substitution model. This is because of the different ionic radii of the dopant In^{3+} (80 pm) and Sr^{2+} (144 pm). Therefore, In^{3+} would be substituted for Ti^{4+} (61 pm), which has a relatively similar ionic size.

Spectroscopic approaches and theoretical calculations are powerful tools for discussing the dopant site. However, direct information on the dopant site in real space has not yet been obtained. An atomic-scale imaging of the dopant element in the crystal lattice should provide clearer evidence. In this type of study, transmission electron microscopy is one of the most effective tools. Currently, the convergence of the electron beam probe in scanning transmission electron microscopy (STEM) can reach subnanometer spatial resolution, enabling the detection of individual single dopants with atom-by-atom imaging.[10–16] Furthermore, STEM techniques coupled with spectroscopic analysis such as energy dispersive x-ray spectroscopy (EDS) can provide atomic-scale imaging and elemental information,[17–20] which will enable us to identify the dopant element with more reliable images. Lu *et al.* reported the dopant-site analysis of samarium-doped $SrTiO_3$ (Sm-STO) lattice via atomic-scale STEM-EDS imaging.[21] Although the atomic-scale elemental mapping demonstrated in ideal model thin-specimens with suitable atomic concentration, confirming the dopant element in actual powder formed samples via STEM-EDS mapping remains difficult. Generally, specimens thickness highly affects delocalization of x-ray emission, which is critical for the quality of atomistic images.[22,23] From this, in particular, prepared thinning specimens suitable for fine TEM and STEM analysis are usually used for atomistic EDS imaging. Thus, atomic-scale EDS imaging for the actual photocatalyst, which is a powder form sample with larger thickness, still be interested. Furthermore, the amount of dopant element is too small to obtain strong enough x-ray signals at the atomic scale.[24,25] To address this matter, applying multivariate statistical analysis (MSA) to a spectral imaging data cube is a promising approach. Principal component analysis (PCA), which is one of the MSA procedures, can reproduce the major spectral information existing in the tiny raw data signal of a single spectrum.[26] Here, principal component vectors, orthogonal to each other, are determined to include more information of various EDS spectra in the spectral imaging data cube. Vectors with lager contribution into main data of spectra have high-order eigenvalues. Then, reconstructing the data cube using only the high-order eigenvalues obtained by the PCA reduces the effects of noise.[27] Namely, thanks to the PCA, we can obtain more reliable spectrum data even with the single pixel. In this study, we tackled the direct atomic-scale confirmation of the indium dopant site in In–STO photocatalyst by using STEM-EDS elemental mapping. By applying the PCA procedure to the data cube of the EDS spectral image, the indium dopant site could be clearly confirmed.

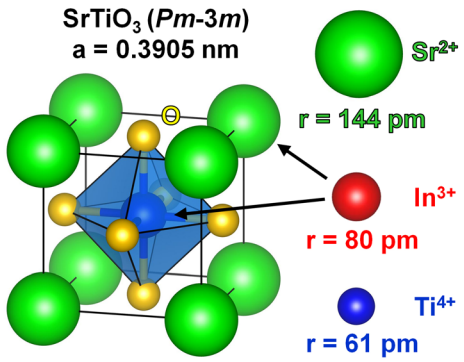

FIG. 1. Crystal structure of $SrTiO_3$ with cubic perovskite structure rendered by using the VESTA program.[29] The lattice constant is $a = 0.3905$ nm. Sr^{2+}, In^{3+}, and Ti^{4+} cations are rendered with green, red, and blue spheres with accurate ionic size ratio, respectively. Numbers below each sphere are the ionic radii of each cation. In^{3+} dopant can substitute for both Sr^{2+} and Ti^{4+} according to charge compensation.

The In–STO material was prepared via a solid-state reaction. $SrCO_3$ (99.9%, Kanto Chemicals) and TiO_2 (99.9%, Kanto Chemicals) were mixed in a Sr/Ti molar ratio of 1.0 and suspended in an $In(NO_3)_3$ (Wako Chemicals) aqueous solution. Here, the ratio In/Ti was 7.1 mol. % for this mixture. The suspension was dried by stirring and then calcined at 1100 °C for 20 h. After calcination, the prepared material was washed with aqueous HCl solution and with pure water to remove any unreacted contaminants and then dried at 80 °C in air for 24 h. Additional details of the material preparation have been described elsewhere.[9] STEM-EDS imaging was performed with a TITAN^3 G2 60–300 (FEI) equipped with a silicon-drift EDS detector (Super-X, FEI) at an acceleration voltage of 300 kV and a screen current of 0.2 nA. The beam convergence angle and sample thickness of this experiment are 21 mrad and more than 400 nm, respectively. The sample thickness is estimated by the particle diameter and shapes of the powder sample, which is also mentioned in previous reports.[9] Elemental mapping was acquired via EDS spectral imaging using the analytical software (Esprit, Bruker) with 128 × 128 pixel resolution at 186 μs of pixel dwell time and 10 eV per channel of energy dispersion in the 0–40 keV energy region. The EDS spectral imaging data cube was acquired by the image integration with about 150 frames (overall acquisition time was 451 s) with drift correcting via Esprit software. Sr-*L*, Ti-*K*, and In-*L* x-ray lines were selected for the reconstruction of each elemental mapping. The STEM-EDS spectral imaging data were converted to an applicable data format that could be treated by digital micrograph software (GMS 2.0, GATAN). PCA was performed by using MSA with the GMS plug-in, which was provided by HREM.[28] The detail results of PCA components for each eigenvalue and examination of artifact were also supplied in Appendix of supplementary material. The reconstruction of the data cube was carried out under the condition of a cumulative variance of 99.2%.

The spatial distribution of the elements in In–STO was imaged by STEM-EDS elemental mapping, as summarized in Fig. 2. The spatial distribution of the indium dopant was clearly observed in the low-

Published under license by AIP Publishing

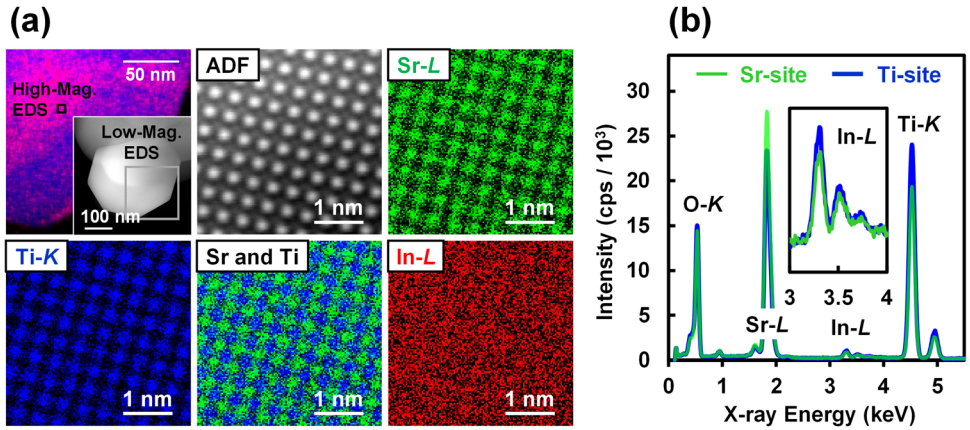

FIG. 2. STEM-EDS spectral imaging of the In–STO sample observed from the ⟨100⟩ zone axis. (a) ADF and elemental mapping images. High-resolution atomic-scale imaging was performed in the square region denoted by the black solid line marked in the low-magnification elemental mapping overwrapped with Ti (blue) and In (red). Atomic column images of Sr-*L*, Ti-*K*, and In-*L* x-ray line intensities are displayed at green, blue, and red colors, respectively. (b) Total EDS spectra extracted from all the Ti sites (blue) and Sr sites (green) in the EDS image with corresponding color. The inset figure is an enlarged In-*L* spectrum.

magnification elemental mapping, which was acquired from the square region of the inset annular dark-field (ADF) image, as shown in Fig. 2(a). Atomic-resolved STEM-EDS elemental mapping was performed in the square region of the image as high-magnification scanning along the $SrTiO_3$ ⟨100⟩ zone axis. The ADF image shows clear atomic column contrast. Elemental mapping of Sr-*L* and Ti-*K* x-ray intensities also exhibited clear contrast of each Sr and Ti atomic column, which are displayed in green and blue, respectively. The Sr and Ti overlay images exhibited alternating features of each atomic column, meaning that Sr- and Ti-site columns can be individually imaged in this elemental mapping. The In-*L* x-ray intensity image (displayed in red) exhibited no typical atomistic contrast, at least in this mapping. This is because only a small amount of In^{3+} dopant exists in this sample; therefore, the x-ray count was too small to image a dopant column using the raw STEM-EDS spectral data. Although the In-*L* x-ray intensity mapping cannot define the dopant site, the total EDS spectra extracted from each Sr site and each Ti site exhibited a clear In-*L* spectrum, as shown in Fig. 2(b). The details of the spectrum-extracted area are shown in the supplementary material, Fig. S1. The enlarged spectra shown in the inset of Fig. 2(b) show that a stronger In-*L* spectrum intensity was more clearly observed at the Ti-site columns than at the Sr-site columns; that is, the In^{3+} dopant preferentially exists at the Ti site. Although the total EDS spectrum analysis indicates that the In^{3+} dopant prefers substitution into Ti^{4+} rather than Sr^{2+}, its substitution by Sr cannot be ruled out. The x-ray delocalization between Sr- and Ti-sites, clearly observed in the spectra, should affect In-*L* spectrum. Namely, we cannot conclude that In dopant site is Ti-site only. Therefore, imaging of the spatial distribution feature of the In^{3+} dopant in the $SrTiO_3$ lattice is needed. To obtain the atomic-scale elemental mapping from the In-*L* x-ray intensity, we performed PCA on the raw STEM-EDS spectral imaging data cube; the reconstructed mapping is summarized in Fig. 3(a). The detailed EDS spectrum after PCA is provided in the supplementary material Fig. S2. The integral x-ray signal intensities were extracted from the EDS spectrum in the energy regions of 1.74–1.94 keV for Sr-*L*, 3.20–3.40 keV for In-*L*, and 4.43–4.63 keV for Ti-*K*. In these elemental mappings, the minimal signal counts were set to zero; that is, the images show the intensity variation corresponding to each atomic column. Sr-*L*, Ti-*K*, and their overlay images clearly show the separation of Sr and Ti atomic columns, as shown in Fig. 2. In addition, the In-*L* x-ray intensity map, as well as the Sr-*L* and Ti-*K* images, clearly shows the atomistic contrast.

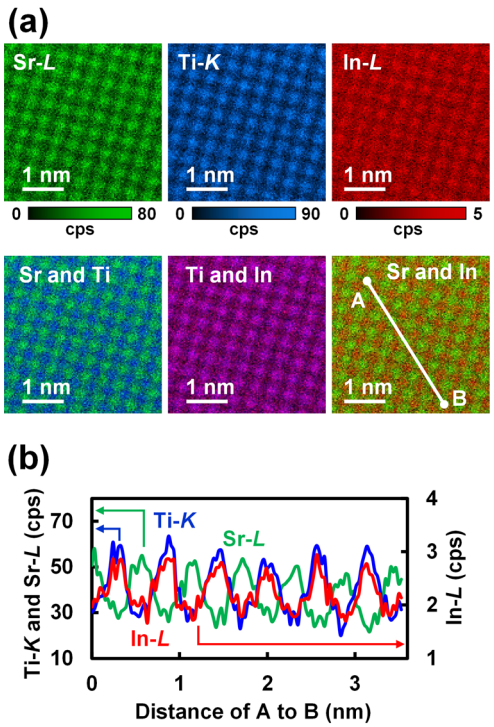

FIG. 3. EDS elemental mapping reconstructed from the spectral imaging data cube processed by using PCA. (a) Sr-*L*, Ti-*K*, and In-*L* x-ray intensity mappings are reconstructed by using integral EDS signal intensities extracted from the 200 eV width energy region for each x-ray peak. (b) X-ray intensity profiles of lines A and B in the Sr and In overlay mapping. Sr-*L*, Ti-*K*, and In-*L* intensity profiles are shown in green, blue, and red solid lines, respectively.

Published under license by AIP Publishing

Therefore, the dopant site of the In–STO sample can be directly confirmed based on these images. Here, the Ti and In overlay images exhibit a single atomistic contrast with a thorough overlap, whereas the atomistic variations in the Sr and In overlay images, as well as those in the Ti and Sr overlay images, have alternating character. These results demonstrate that the dopant site of In^{3+} should be Ti^{4+}. The x-ray intensity profiles of the A–B lines in the Sr and In overlay images, displayed in Fig. 3(b), show the above-mentioned results more clearly. The atomistic features of the Ti-*K* (blue) and In-*L* (red) x-ray profiles are identical. However, the Sr-*L* (green) and In-*L* x-ray intensity curves are throughly separated, and no atomistic characteristics of In-*L* x-ray intensities were observed at any Sr site. These results strongly support the In^{3+} substitution model of Eq. (1) rather than Eq. (2), which is in good agreement with previous research.[9] As explained in the Appendix of the supplementary material, by through the PCA procedure, the spatial information of In-*L* signals is interpreted to the side of Ti-site, which was clearly separated from Sr-site. This is a reason for clear reconstructed of In atomic column as Ti-site. The In atoms can be seen at every Ti atomic column of provided EDS mapping. This should not be caused by the particularly concentrating of In in observed area, but the large sample thickness. Namely, dopant sites are more averaged toward the atomic column direction and can be observed every Ti atomic columns. Indeed, the signal intensities of In against Ti or Sr as shown in the line profiles of Fig. 3(b) are considerably small, and the intensity ratio is simply estimated as 4–5%. Thus, the remarkable concentrating of dopant should be negligible. Based on the ionic radius of each cation, In^{3+} (80 pm) and Ti^{4+} (61 pm) substitution should be better than In^{3+} and Sr^{2+} (144 pm) substitution. Here, we provide direct information on In^{3+} and Ti^{4+} substitution from atomic-scale imaging, verifying the O^{2-} vacancy formation model as a doping mechanism of In–STO. This should contribute to further studies on metal-cation-doped photocatalysts.

In conclusion, we confirmed the doping mechanism of the In–STO photocatalyst by direct atomic-scale imaging of STEM-EDS elemental mapping. The as-prepared In–STO sample doped at In/Ti = 7.1 mol. % was observed by STEM-EDS spectral imaging, and a clear atomistic contrast of Sr and Ti was obtained. The total EDS spectrum extracted from all the Ti-site columns and Sr-sites columns in the EDS image exhibited a higher In-*L* x-ray spectrum intensity at the Ti site than at the Sr site. By applying PCA to the STEM-EDS spectral imaging data cube, the indium dopant site was directly imaged by In-*L* x-ray intensity mapping. The indium site thoroughly overlapped with the Ti site and was completely separated from the Sr site. This imaging feature provides direct evidence of the doping mechanism of In–STO as Ti^{4+}–In^{3+} substitution with O^{2-} vacancy formation. The direct imaging of dopant elements by atomic-scale STEM-EDS spectral imaging coupled with PCA should significantly contribute to various fields of research in metal-cation doping materials as well as photocatalysts.

See the supplementary material Appendix of PCA, details of total Ti- and Sr-site spectra extraction, and comparison of EDS spectrum before and after PCA are available in the supplementary material.

AUTHORS' CONTRIBUTIONS

M.K. performed the STEM and STEM-EDS experiments and analyses. N.T. performed the MSA and PCA for the original spectral imaging data. H.S. performed the sample preparation. All authors contributed to the preparation of the manuscript and approval of this study.

H.S. is an International Research Fellow of the Japan Society for the Promotion of Science (JSPS). The authors acknowledge funding from JSPS KAKENHI (Grant Nos. JP18F18029, JP18KK0161, and JP19H00915). We would like to thank Editage (www.editage.com) for English language editing.

DATA AVAILABILITY

The data that support the findings of this study are available within the article and its supplementary material.

REFERENCES

[1]K. Domen, S. Naito, M. Soma, T. Onishi, and K. Tamaru, J. Chem. Soc. **1980**, 543.
[2]Y. Ham, T. Hisatomi, Y. Goto, Y. Moriya, Y. Sakata, A. Yamakata, J. Kubota, and K. Domen, J. Mater. Chem. A **4**, 3027 (2016).
[3]T. H. Chiang, H. Lyu, T. Hisatomi, Y. Goto, T. Takata, M. Katayama, T. Minegishi, and K. Domen, ACS Catal. **8**, 2782 (2018).
[4]Y. Sakata, Y. Miyoshi, T. Maeda, K. Ishikiriyama, Y. Yamazaki, H. Imamura, Y. Ham, T. Hisatomi, J. Kubota, and A. Yamakata, Appl. Catal. A **521**, 227 (2016).
[5]Q. Wang, T. Hisatomi, Q. Jia, H. Tokudome, M. Zhong, C. Wang, Z. Pan, T. Takata, M. Nakabayashi, and N. Shibata, Nat. Mater. **15**, 611 (2016).
[6]Y. Goto, T. Hisatomi, Q. Wang, T. Higashi, K. Ishikiriyama, T. Maeda, Y. Sakata, S. Okunaka, H. Tokudome, and M. Katayama, Joule **2**, 509 (2018).
[7]T. Takata and K. Domen, J. Phys. Chem. C **113**, 19386 (2009).
[8]Y. Kim, M. Watanabe, A. Takagaki, J. Matsuda, and T. Ishihara, ChemCatChem **11**, 6270 (2019).
[9]H. Sudrajat, M. M. Fadlallah, S. Tao, M. Kitta, N. Ichikuni, and H. Onishi, Phys. Chem. Chem. Phys. **22**, 19178 (2020).
[10]P. M. Voyles, D. A. Muller, J. L. Grazul, P. H. Citrin, and H.-J. L. Gossmann, Nature **416**, 826 (2002).
[11]P. M. Voyles, J. L. Grazul, and D. A. Muller, Ultramicroscopy **96**, 251 (2003).
[12]S. Wang, A. Y. Borisevich, S. N. Rashkeev, K. Sohlberg, M. V. Glazoff, S. J. Pennycook, and S. T. Pantelides, Nat. Mater. **3**, 143 (2004).
[13]S. H. Oh, K. van Benthem, S. I. Molina, A. Y. Borisevich, W. Luo, P. Werner, N. D. Zakharov, D. Kumar, S. T. Pantelides, and S. J. Pennycook, Nano Lett. **8**, 1016 (2008).
[14]K. Kimoto, R.-J. Xie, Y. Matsui, K. Ishizuka, and N. Hirosaki, Appl. Phys. Lett. **94**, 041908 (2009).
[15]S.-Y. Choi, S.-Y. Chung, T. Yamamoto, and Y. Ikuhara, Adv. Mater. **21**, 885 (2009).
[16]R. Ishikawa, N. Shibata, T. Taniguchi, and Y. Ikuhara, Phys. Rev. Appl. **13**, 034064 (2020).
[17]G. Kothleitner, J. Neish, M. R. Lugg, N. D. Findlay, S. W. Grogger, F. Hofer, and L. J. Allen, Phys. Rev. Lett. **112**, 085501 (2014).
[18]P. Lu, L. Zhou, M. J. Kramer, and D.,J. Smith, Sci. Rep. **4**, 3945 (2014).
[19]B. Feng, T. Yokoi, A. Kumamoto, M. Yoshiya, Y. Ikuhara, and N. Shibata, Nat. Commun. **7**, 11079 (2016).
[20]P. Gao, R. Ishikawa, B. Feng, A. Kumamoto, N. Shibata, and Y. Ikuhara, Ultramicroscopy **184**, 217 (2018).
[21]P. Lu, E. Romero, S. Lee, J. L. MacManus-Driscoll, and Q. Jia, Microsc. Microanal. **20**, 1782 (2014).
[22]Z. Chen, M. Weyland, X. Sang, W. Xu, J. H. Dycus, J. M. LeBeau, A. J. D'Alfonso, L. J. Allen, and S. D. Findlay, Ultramicroscopy **168**, 7 (2016).
[23]P. Lu, J. M. Moya, R. Yuan, and J. M. Zuo, Ultramicroscopy **186**, 23 (2018).
[24]M. Watanabe and D. B. Williams, Ultramicroscopy **78**, 89 (1999).
[25]M. Watanabe, D. B. Williams, and Y. Tomokiyo, Micron **34**, 173 (2003).
[26]P. G. Kotula, D. O. Klenov, and H. S. von Harrach, Microsc. Microanal. **18**, 691 (2012).
[27]See https://analyticalscience.wiley.com/do/10.1002/micro.483/full/ for "information about theoretical and procedure details of PCA" (last accessed January 28, 2021).
[28]See https://www.hremresearch.com/Old/index.html for "information about software details of MSA plug-in by HREM" (last accessed January 28, 2021).
[29]K. Momma and F. Izumi, J. Appl. Crystallogr. **44**, 1272 (2011).

Published under license by AIP Publishing